

Understanding NLR in Seyfert Galaxies: numerical simulation of jet-cloud interaction

P. Rossi¹, A. Capetti¹, G. Bodo¹, S. Massaglia², and A. Ferrari^{1,2}

¹ Osservatorio Astronomico di Torino, I-10025 Pino Torinese, Italy
email: rossi@to.astro.it, capetti@to.astro.it, bodo@to.astro.it

² Dipartimento di Fisica Generale dell'Università, Via Pietro Giuria 1, I-10125 Torino, Italy
email: massaglia@ph.unito.it, ferrari@ph.unito.it

Received / Accepted

Abstract. Recent HST observations suggest that the NLR in Seyfert Galaxies can be the result of interaction between jet and external inhomogeneous medium; following this suggestion we perform numerical simulations considering the impact of a radiative jet on a dense cloud. We approach the problem adopting a hydrodynamical code, that consents us to study in detail the jet hydrodynamics, while we choose a more simplified treatment of radiative processes, in order to give a qualitatively good interpretation of the emission processes. Our three main purposes are: i) to reproduce in our simulations the physical conditions observed in the NLR of Seyfert Galaxies, ii) to obtain physical constraints of the jet parameters and iii) to study the jet capacity to photoionize the surrounding medium.

We find that the jet-cloud interaction leads to clumps of matter with density, temperature and velocity that agree with observations. Conversely, the photoionizing flux radiated by the jet-induced shocks does not appear to be sufficient to account for the NLR line luminosity but it may produce local and transient effects on the NLR ionization balance.

Finally, the observational requirements can be matched only if jets in Seyfert galaxies are relatively heavy, $\rho_{\text{jet}} \gtrsim 1 \text{ cm}^{-3}$, and with velocities smaller than $\lesssim 50,000 \text{ km s}^{-1}$, very different from their counterparts in radio-galaxies.

Key words: Hydrodynamics – ISM: jets and outflows – NLR in Seyfert Galaxies

1. Introduction

Extensive HST emission-line imaging of Seyfert galaxies has for the first time resolved details of the structure of their Narrow Line Regions (NLR). In several cases cone-like morphologies have been revealed, similar in shape to - but of much smaller linear extent than - the Extended Narrow Line Regions (ENLR) seen in the lower resolution ground based images (Wilson & Tsvetanov, 1994 and references therein). In the standard model of the NLR, the UV emission of the nucleus is responsible of photoionizing the Interstellar Medium (ISM) of the host galaxy. These conical distributions of the ionized gas have been interpreted as a confirmation of the anisotropy of the nuclear radiation field which, in the framework of the unified scheme for Seyfert galaxies (e.g. Antonucci 1993) is caused by the shadowing of an obscuring circumnuclear torus. However, in galaxies with linear radio structures, the morphology of the emission-line region appears to be directly related to that of the radio emission. In particular, in Seyferts with radio jets (e.g. Mrk 3, Mrk 348, Mrk 6, Mrk 1066, ES0 428-G14), the NLR itself appears jet-like and is spatially coincident with the radio jet, while the emission-line region takes a different form when a radio lobe is present (e.g. Mrk 573, Mrk 78, NGC 3393): arc-like shells of emission, very reminiscent of bow-shocks, surround the leading edge of the lobes (Capetti et al. 1995a, 1995b, 1996; Falcke et al. 1996, 1998). This dichotomy in radio and emission-line morphology is reflected in their different scales: bow-shock structures cover several kiloparsecs, while the jet-like features extend only over a few hundred parsecs. The simplest interpretation of this radio-to-optical correspondence is that the radio emitting outflow creates an expanding and cooling gas halo. The compression induced by the outflow causes the line emission to be highly enhanced in the regions where the jet-cloud interactions occur. A clear confirmation of this scenario came recently from HST spectroscopy of Mrk 3 (Capetti

et al. 1999): its NLR has velocity field characteristic of a cylindrical shell expanding at a rate of 1700 km/s. They interpreted this as the consequence of the rapid expansion of a hot gas cocoon surrounding the radio-jet, which compresses and accelerates the ambient gas.

HST observations also provided evidence for spatial variations in the NLR ionization structure. In NGC 1068 the material located along the radio jet is in a much higher ionization state than its surroundings. This might suggest the presence of a local source of ionization which dominates over the nuclear radiation field (Capetti, Axon and Macchetto 1997; Axon et al. 1998). In other sources, too distant for such a detailed analysis, the radial variations of the ionization parameter are generally much flatter than expected from pure nuclear photoionization on the basis of the measured density gradients (Capetti et al. 1996, Allen et al. 1999) requiring again a local source of ionizing photons. An appealing possibility of interpreting these data is to invoke the ionizing effects of shocks, originated by jet-cloud interactions: if these shocks are fast enough (velocities $>$ a few hundred km s⁻¹) the hot, shocked gas could produce a significant flux of ionizing photons (Sutherland, Bicknell and Dopita 1993; Dopita and Sutherland 1995, 1996). Direct evidence for this emission has been found by Axon, Capetti and Macchetto (1999) who showed that the radio-jets in the Seyfert 2 galaxies Mrk 348 and Mrk 3 are associated with an extended linear structure in UV and optical continua. In this picture, the radio-jet would not only determine the morphology of the NLR but is physically involved in its ionization. A radio imaging survey of the CfA sample of Seyfert (Kukula et al. 1995) shows that radio linear structures are present in a large fraction of sources (more than 50%) suggesting that such an interaction is likely to be a quite common phenomenon in this class of objects.

The jet interaction with the external medium is clearly a complex physical problem which involves both a hydrodynamical study of the jet propagation as well as a detailed understanding of the microphysics of the induced shocks, which might also be magnetized, and of the radiative processes.

In the framework of Seyfert galaxies this issue has been tackled by several authors (Dopita and Sutherland 1995, 1996, Evans et al. 1999, Wilson and Raymond 1999, Allen et al. 1999). Their focus is however mainly on the shocks properties with a very detailed treatment of the emission mechanisms, with simplifying assumptions about the hydrodynamics (e.g. plane parallel geometry, steady-state shock). The comparison with the observations is based on the emitted spectrum and in particular on diagnostic line-ratios, particularly with the aim of distinguishing the different signatures of nuclear versus local photoionization.

In this paper we follow a complementary, albeit different, approach by studying in detail the jet hydrodynamics, while adopting a simplified treatment of the radiative

processes, as we employ an equilibrium cooling function in an optically thin approximation. This approach allows us to compare the results of simulations with the observed properties of NLR, in particular their morphology, the expansion velocities and the characteristic values of gas density and temperature. More precisely we consider the interaction of the jet with an inhomogeneity in the external medium (cloud) and our aim is that of constraining the jet and cloud physical parameters for which it is possible to reproduce the observed conditions. In this way, in addition of getting a better understanding of the NLR physics, we can also obtain information on the jet properties from the NLR data. Moreover, we can calculate the fraction of the jet power converted in radiation by shocks, resulting from the interaction of the jet with the environment. We then get from the global dynamics a conversion efficiency from kinetic to radiative power and we can determine whether the jet itself, via shocks, can provide an *in situ* photoionization source for the NLR emitting material, as discussed above.

Steffen et al. (1997a) have used a rather similar approach with the main difference that they considered the jet propagating into a uniform medium. It seems that in this situation it is impossible to reach the high densities typical of the NLR with jet-like emission (see discussion below) on which we will focus in the present paper. This is because, at low density, radiation is not efficient enough to give the needed compression factors. The conditions of the emitting material obtained by Steffen et al. seem to be appropriated for the case of the more extended (lobe-like) line emission structure.

Steffen et al. (1997b) considered also jet-cloud interactions mainly from an analytical point of view. They found that when a jet interacts with a large number of clouds the most relevant effects on the NLR structure are due to the most massive clouds located along the jet path. This lead us to our choice for the geometry of the simulation in which the jet hits a single dense cloud.

The paper is structured as follows: In the next section (Sect. 2), we describe the basic physical problem and the observational constraints, while the equations used and the method of solution are examined in Sect. 3 and 4; the results of simulations are discussed in Sect. 5; conclusions are drawn in Section 6.

2. Observational data and astrophysical scenario

Observational data provide us with quite detailed information on the physical conditions of the narrow line emitting regions, in particular HST observations can now be used to determine the properties of individual NLR clouds: typically, densities are larger than 10³ cm⁻³, temperatures are of the order of 10⁴ – 2 × 10⁴ K, and velocities are ~ 300 – 1000 km s⁻¹ (Caganoff et al. 1991, Kraemer, Ruiz and Crenshaw 1998, Ferruit et al. 1999, Axon et al. 1998, Capetti et al. 1999).

These are the observational constraints that we try to match in our simulations. Results of simulations of a jet impinging on a uniform medium, with properties typical of the ISM, have shown that it is not possible to match, in this situation, the density values reported above (Steffen et al. 1997a, Rossi & Capetti 1998). We will therefore consider throughout the rest of the paper the case of a jet impinging on pre-existing inhomogeneities. We can identify such inhomogeneities with giant molecular clouds (GMCs), that typically populate spiral galaxies. These objects have typically mass $\sim 10^5 - 10^6 M_\odot$, radius $\lesssim 100$ pc, and temperature ~ 10 K (Blitz 1993). The resulting particle densities span from a few up to about hundred particles per cm^3 .

A supersonic jet, of radius ~ 10 pc, that bore its way through the interstellar medium has a considerably good chance of impinging frontally upon a (much larger) GMC, and this is the case we will consider in our simulations. In any event, this latter case, i.e. the head-on collision with a large cloud, can be considered the most efficient case of interaction, for the compression, acceleration and heating of the NLR material.

As discussed below the effects of the jet/cloud interaction last for a time considerably longer than the cloud crossing time. Moreover, the jet crosses the tenuous inter-cloud regions at a much higher speed than while in a cloud. We therefore expect that more than one cloud will be interacting at any given time and they will display simultaneously the different evolutionary stages of the interaction.

3. The physical problem

We study the evolution of a cylindrical fluid jet impinging upon a cold heavy steady inhomogeneity, namely the cloud, in pressure equilibrium with the external medium. The relevant equations governing the jet evolution, for mass, momentum conservation, and radiative losses, are

$$\frac{\partial \rho}{\partial t} + \nabla \cdot (\rho \mathbf{v}) = 0, \quad (1a)$$

$$\frac{\partial \rho v_r}{\partial t} + \nabla \cdot (\rho v_r \mathbf{v}) = -\frac{\partial p}{\partial r}, \quad (1b)$$

$$\frac{\partial \rho v_z}{\partial t} + \nabla \cdot (\rho v_z \mathbf{v}) = -\frac{\partial p}{\partial z}, \quad (1c)$$

$$\frac{\partial E}{\partial t} + \nabla \cdot (E \mathbf{v}) = -p \nabla \cdot \mathbf{v} - \mathcal{L}, \quad (1d)$$

where the fluid variables p , ρ , \mathbf{v} and E are, as customary, pressure, density, velocity, and thermal energy ($p/(\Gamma - 1)$) respectively; Γ is the ratio of the specific heats; \mathcal{L} represents the radiative energy loss term (energy per unit volume per unit time, Raymond and Smith 1977).

The jet occupies initially a cylinder of length L . The initial flow structure has the following form:

$$v_z(r) = \begin{cases} \frac{v_z(r=0)}{\cosh[(r/a)^m]} & z \leq L \\ 0 & z > L \end{cases}$$

where m is a ‘steepness’ parameter for the shear layer separating the jet from the external medium (see Fig. 1). The choice of separating the jet’s interior from the ambient medium with a smooth transition, instead of a sharp discontinuity, avoids numerical instabilities that can develop at the interface between the jet and the exteriors, especially at high Mach numbers.

Regarding the cloud, we fix its initial density ρ_{cloud} and impose pressure equilibrium with respect to external medium; for simplicity we consider a steady cloud, with a thickness equal to the jet diameter.

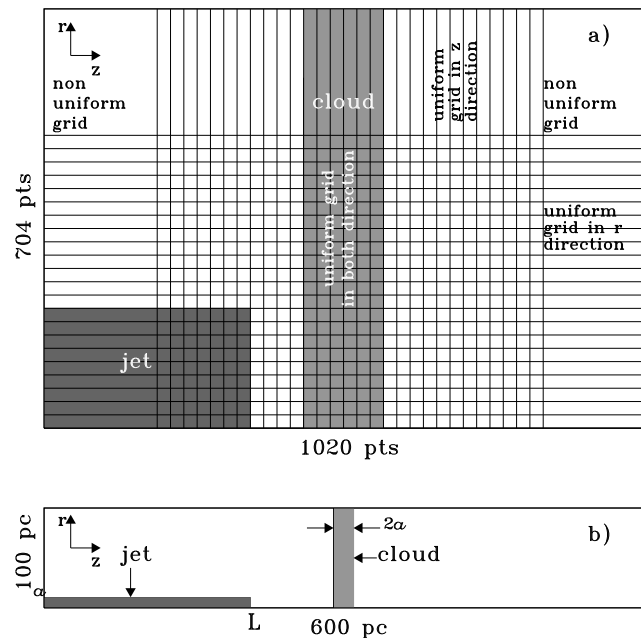


Fig. 1. In panel a) the computational domain is sketched. The grid is finer on the region of jet/cloud interaction, while is coarser far from the region of our interest. In panel b) the physical domain is shown.

4. The numerical scheme

4.1. Integration domain and boundary conditions

Integration is performed in cylindrical geometry and the domain of integration ($0 \leq z \leq D$, $0 \leq r \leq R$) is covered by a grid of 1020×704 grid points. The axis of the beam is taken coincident with the bottom boundary of the domain ($r = 0$), where symmetric (for p , ρ and v_z) or antisymmetric (for v_r) boundary conditions are assumed. At the top boundary ($r = R$) and right boundary ($z = D$) we choose free outflow conditions, imposing for every variable Q null gradient ($dQ/d(r, z) = 0$). The boundaries are placed as far as possible from the region of the jet where the most interesting evolutionary effects presumably take

place by employing a nonuniform grid both in the longitudinal (z) and the radial (r) directions (Fig. 1, panel a)). In the radial direction the grid is uniform over the first 500 points and then the mesh size is increased assuming $\Delta r_{j+1} = 1.015\Delta r_j$. The jet spans over 200 uniform meshes, while the external boundary is shifted to $r = 10a$ where a is the jet radius. As for the z -direction, we assume a constant fine grid in the central part of the domain, where the cloud is located, i.e. in a sub-domain of length $40a$, between the grid points 180 and 844; conversely, in the remaining part we consider an expanded grid increasing the mesh distance according to the scaling law $\Delta z_{j\pm 1} = 1.015\Delta z_j$, where the minus sign applies in the first 180 grid points and the plus sign above grid point 844.

4.2. Integration method

The basic equations (1a-d) have been integrated with a two-dimensional version of the Piecewise Parabolic Method (PPM) of Colella & Woodward (1984) (for a discussion of the main characteristics of this code and its merits for this kind of problems see Bodo et al. 1995). Radiative losses are dealt with the operator splitting technique, following which we split a single time step into two parts. In the first part, we advance the dynamical quantities, by using the adiabatic equations. In the second part we update the internal energy, keeping all the other variables constant, by taking into account radiative losses.

4.3. Physical parameters and Scaling

The physical problem that we are approaching is quite complex, with three different interacting and radiating media, i.e. jet, ambient medium and cloud, each one described by its density, temperature, velocity and size. We note that in the adiabatic simulations of propagating jets, by normalizing to the jet density, sound speed, jet radius and sound crossing time over the jet radius, we are left with only two parameters, namely the density ratio between jet and external medium and the jet Mach number. The presence of radiation complicates the matter (Rossi et al. 1997), in fact temperature is not scale free, since the radiative loss function in Eq. (1c) explicitly depends on its physical value and in addition to the sound crossing time ($t_{\text{cr}} = a/c_s$), we have another typical time scale of the system, i.e. the radiative time scale, defined as $t_{\text{rad}} = p/[(\Gamma - 1)\mathcal{L}]$ which depends on the density of the medium. Therefore in this case one has to consider for each medium the value of density and temperature as independent parameters. In addition, as we already noticed we are now considering three media. When the jet passes through the cloud, the evolution of the compressed cloud material is completely different with respect to the case of two media, where the jet continues to push dense material at the head and it does not have any reaccelerations re-

lated to the passage from a denser to lighter medium. We would like to stress that the presence of an inhomogeneity is fundamental, in fact only in this case, as we show later, it is possible to reach the proper density for the emitting material. In conclusion, we must assign a large number of physical parameters for defining the initial conditions of our simulations.

A thorough investigation of such huge parameter space is unfeasible; however, not all the parameters are equally important and some of them can be well constrained by observational considerations. As a first step we will then fix criteria to minimize the number of free parameters.

Concerning the external (uniform) medium, we have to fix ρ_{ext} and T_{ext} , having $v_{\text{ext}} = 0$. With respect to ρ_{ext} , we can assume one particle per cubic centimeter, a value which we know to be appropriate to the interstellar medium of our Galaxy (Cox & Reynolds, 1987). In reference to T_{ext} , again its choice is not so crucial, since the most important temperature for the emission processes is the shock temperature, depending mainly on jet velocity, in any case observations tell us that the external medium is completely ionized, which means temperatures larger than 10^4 K, and we assume $T_{\text{ext}} = 10^4$ K.

The jet is physically described by its density ρ_{jet} , temperature T_{jet} , initial velocity v_{jet} and radius a . The radius a can be chosen as our length unit in order to scale the other lengths in the system, and following the radio observational suggestions (Pedlar et al. 1993, Kukula et al. 1999) we consider it to be 10 pc. Concerning the jet density we do not have any tightening constraint, so in a first approach, we take it equal to ρ_{ext} . Relatively to T_{jet} , looking at the loss function (Fig. 2) we can immediately realize that its initial value it is not so crucial, since cooling is fast and soon the jet temperature falls to $\sim 10^4$ K. Anyway T_{jet} in our simulations is taken to be 10^6 K. The jet velocity will be instead an important parameter of our simulations.

Finally we consider the cloud, its density ρ_{cloud} is the parameter on which we will focus our investigation. T_{cloud} will be fixed by imposing pressure equilibrium with the external medium. Actually GMC's are not required to be in pressure equilibrium since they might be autogravitating, however, as discussed for the external temperature, the exact value of T_{cloud} is not crucial for the results of the simulations. For simplicity we consider a steady cloud ($v_{\text{cloud}} = 0$). The cloud dimensions must lie in the range of GMCs, so we will fix the size longitudinal to the jet to 20 pc (i.e. $2a$), with a indefinitely large (with respect to a) transversal size.

In summary, we have three control parameters, namely the initial cloud density, the initial jet velocity and the initial jet density, that we fix equal to one particle per cm^{-3} . So we will investigate in details the effects of adopting different values for v_{jet} and ρ_{cloud} .

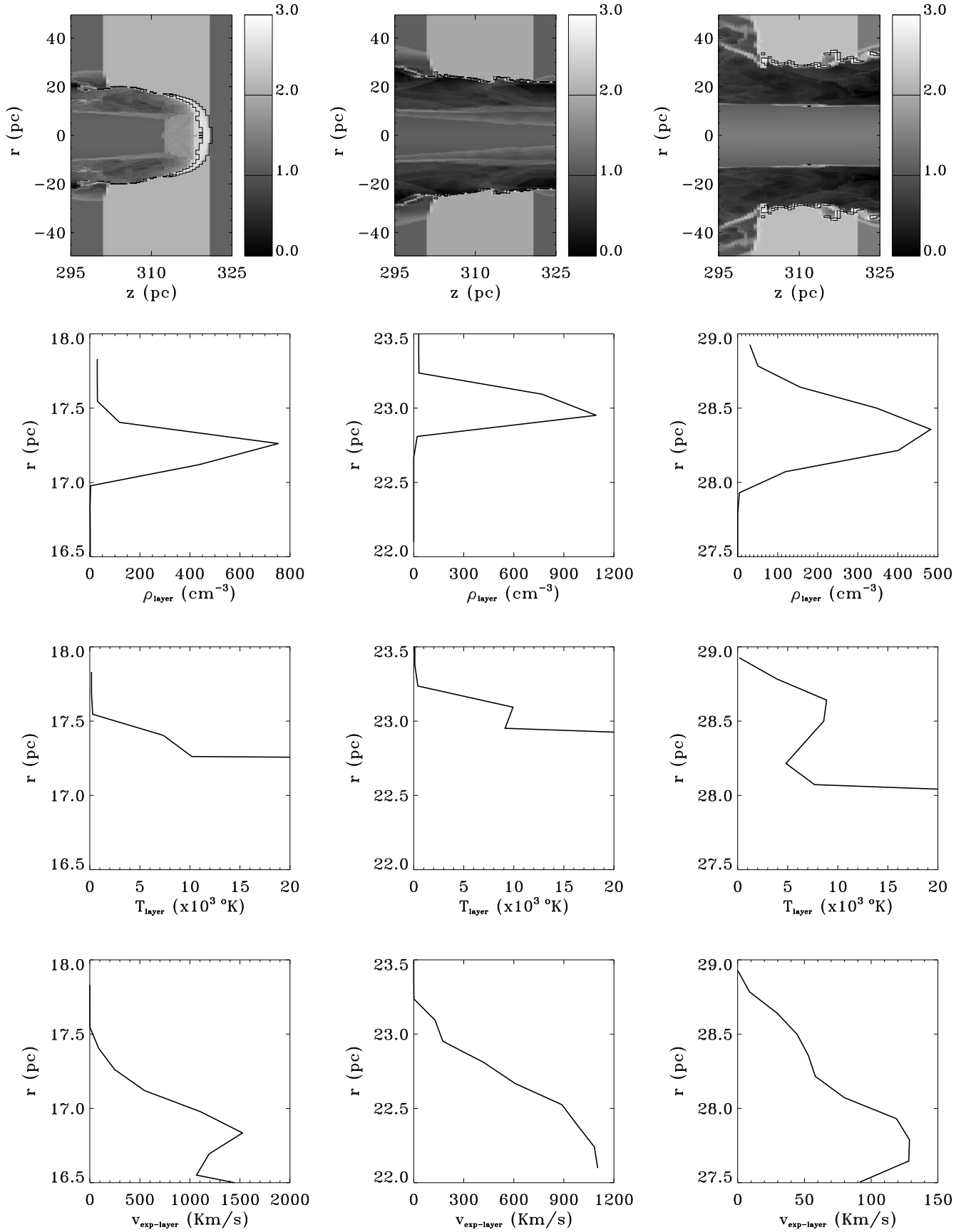


Fig. 3. Images of the density distribution showing the jet-cloud interaction and cuts of density, temperature and expansion velocity, in the middle of the cloud, across the thin layer of compressed material for the case $\rho_{\text{cloud}} = 30 \text{ cm}^{-3}$, $v_{\text{jet}} = 6500 \text{ km s}^{-1}$, at different times. The three columns correspond respectively to $t = 1 t_{cc}$, $t = 2 t_{cc}$ and $t = 5 t_{cc}$.

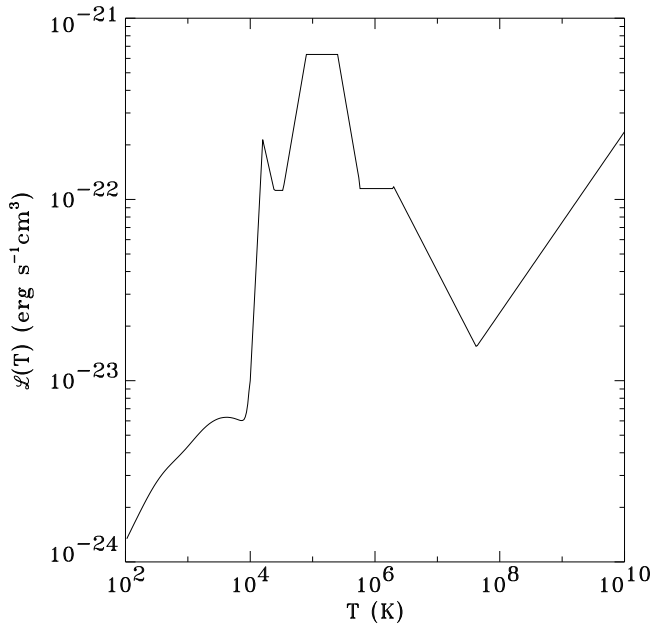


Fig. 2. Plot of the energy loss function vs temperature (Raymond & Smith 1977).

5. Results

We begin our discussion with a short general description of the complete evolution of the jet-cloud interaction, that can be summarized in three steps (see Fig. 3 for a visualization of the basic features of the three steps for the case $\rho_{\text{cloud}} = 30 \text{ cm}^{-3}$ and $v_{\text{jet}} = 6500 \text{ km s}^{-1}$):

- The jet hits the cloud, forming a strong shock, the post-shock region becomes hot and blows up, because of its increasing pressure; the jet material is conveyed in a back-flow that squeezes the jet itself. During this process the cloud material is compressed and heated by the shock, at the head the temperature is very high ($> 10^8 \text{ K}$), while on the jet sides it is lower $\sim 10^7 \text{ K}$, so that it can cool down, to reach the observed line emission conditions. It is in this region, forming a layer around the jet, that the narrow line emission can originate. Our analysis will therefore concentrate on the properties of this region. During this first phase, in which the jet crosses the cloud, the layer is accelerated by the strong inside pressure and cools down, its density thereby increases (see the leftmost panels in Fig. 3).

- The second phase begins when the jet is completely out of the cloud, the compressed emitting material reaches a quasi-steady state, during which the emission is almost constant, the inside pressure begins to decay, but the emitting layer is still accelerated. From Fig. 3 (central panels), we can see that the material in the layer has been compressed, its maximum density has increased, while its temperature has decreased. The maximum density is found

now at temperatures around 10^4 K , and its velocity has also increased.

- In the third phase, the inside pressure has decayed and the emitting layer begins to slow down, the jet flows freely through the cloud and also the emission decreases, eventually disappearing. From Fig. 3 (rightmost panels), we see a decrease in density and velocity, while almost all the layer is found at $5 \times 10^3 < T < 10^4 \text{ K}$.

The efficient formation of the line emitting region will therefore depend on the efficiency of radiation during the jet crossing of the cloud. We will then introduce two typical timescales, the *cloud crossing time* and the *radiative time*, whose ratio will be a fundamental parameter for determining the evolution of the narrow line emitting layer. Following analytical treatments of the jet-ambient interaction we define the cloud crossing time as $t_{\text{cc}} = d(1 + \sqrt{\rho_{\text{cloud}}/\rho_{\text{jet}}})/v_{\text{jet}}$, where we have assumed, for the jet head velocity in the cloud, the steady velocity obtained from the 1-D momentum balance in a medium with $\rho = \rho_{\text{cloud}}$ (see, e.g., Cioffi and Blondin 1992, Norman et al. 1982). In this way we are actually overestimating the crossing time, since our situation is not steady, however this value is sufficiently accurate for our purposes. Concerning the radiative time, its definition is given in Section 4.3, however, we must notice that for its evaluation we have to assume a value for the temperature, in the following considerations we have taken $T = 10^7 \text{ K}$, that is the average of the typical post-shock temperature in the region of our interest, this choice is properly done for all jets with $v_{\text{jet}} = 6500 \text{ km s}^{-1}$ and $v_{\text{jet}} = 32500 \text{ km s}^{-1}$, while it is overestimated for the low velocity cases, that means that t_{rad} for those cases are shorter than the real ones. We have then defined $\tau \equiv t_{\text{cc}}/t_{\text{rad}}$ as the ratio between crossing and radiative time scales and this, as said before, is an important parameter for the interpretation of the results.

As a first step in our analysis, we have performed an exploration of the parameter space. As discussed before, we reduced our parameters to ρ_{cloud} and the initial v_{jet} . In Table 1 we report, for each pair of their values, typical values of density, expansion velocity and temperature of the emitting material and the value of τ . The density is the median value of density distribution weighted on the emissivity function (that is proportional to ρ^2), while velocity and temperature are those corresponding to this density value. All the quantities are evaluated at $2t_{\text{cc}}$, this choice is due to the fact that during this period the expansion velocity of the emitting material increases rapidly reaching a maximum and then decreases monotonically, so that, if the expansion velocity does not match the observational constraint within this time, it never will, and the case will not be of interest for our analysis. Radiation must therefore act efficiently during this time, in order to create the needed conditions for radiation, and this poses a lower limit on the value of τ . On the basis of the values reported

in this table we choose the most promising cases for our investigation.

Table 1. Parameters of the simulations

	$v_{jet} =$ 1300 $km\ s^{-1}$	$v_{jet} =$ 6500 $km\ s^{-1}$	$v_{jet} =$ 32500 $km\ s^{-1}$
$\rho_{cloud} =$ 30 cm^{-3}	430 cm^{-3} 23 $km\ s^{-1}$ 8,900 K $\tau = 1.75$	1130 cm^{-3} 335 $km\ s^{-1}$ 9,600 K $\tau = 0.34$	31 cm^{-3} 6 $km\ s^{-1}$ 23,500 K $\tau = 0.06$
$\rho_{cloud} =$ 60 cm^{-3}	$\tau = 4.65$	1170 cm^{-3} 100 $km\ s^{-1}$ 8,300 K $\tau = 0.93$	390 cm^{-3} 380 $km\ s^{-1}$ 21,500 K $\tau = 0.17$
$\rho_{cloud} =$ 120 cm^{-3}	$\tau = 13.2$	1360 cm^{-3} 170 $km\ s^{-1}$ 10,500 K $\tau = 2.64$	1690 cm^{-3} 722 $km\ s^{-1}$ 11,300 K $\tau = 0.5$

Considering the first column we can immediately realize that jets at low velocity cannot reach conditions comparable to those observed. The values of τ for these simulations are high, meaning that radiation is very efficient. On the other hand, the jet momentum is low and cannot drive the emitting material at high velocities. For the case $\rho_{cloud} = 30\ cm^{-3}$ we have, in fact, high densities in accord with the high value of τ , but very low velocities. For this reason we did not perform simulations for the other two cases of higher density, since jets would produce stronger and cooler compression practically at rest, very far from the observational scenario.

Looking at the high velocity case, we see that, in the case of small inhomogeneities, τ has a very low value and, therefore, radiation is inefficient. The jet is very energetic and sweeps the cloud, before radiation becomes effective and so it does not form any condensation (the velocity reported for this case is therefore meaningless). Increasing the cloud density, we increase also the value of τ : the maximum density increases, but it is still quite low. Only for the high density cloud ($\tau = 0.5$), we get values of density and velocity in agreement with observations.

Regarding the intermediate velocity, the values of τ are > 0.3 : radiation is efficient and thus the emitting layer can reach sufficiently high densities. Only in the lighter cloud

case, however, the velocity is comparable to the observed values.

From this exploration of the parameter space we can conclude that the observed conditions can be matched only for a narrow range of parameters and that the properties of the emitting layer depend essentially only on one parameter, the ratio between the radiative timescale and the cloud crossing timescale τ . For low values of τ ($\tau < 0.3$), radiation is inefficient and the densities in the layer are too low. For higher values of τ ($\tau > 0.55$) we find, on the other hand, that the velocity of the emitting layer becomes too small. This is because the cloud density is high and the jet momentum flux is too small to impart to it a large enough velocity. Only for a narrow range of values of τ we can match the observed conditions and, in Table 2, we have translated these limits into limits on velocity range at different cloud densities.

Table 2. Ranges of jet velocities that can match the observed properties

	$0.3 < \tau < 0.55$
$\rho_{cloud} = 30\ cm^{-3}$	$4,000\ km\ s^{-1} < v_{jet} < 7,500\ km\ s^{-1}$
$\rho_{cloud} = 60\ cm^{-3}$	$11,000\ km\ s^{-1} < v_{jet} < 20,500\ km\ s^{-1}$
$\rho_{cloud} = 120\ cm^{-3}$	$30,000\ km\ s^{-1} < v_{jet} < 55,500\ km\ s^{-1}$

5.1. Case of $\rho_{cloud} = 120\ cm^{-3}$, $v_{jet} = 32500\ km\ s^{-1}$

In this subsection we will discuss in more details the case that best matches the observational scenario. We begin our discussion showing, Fig. 4, a gray-scale image with a snapshot of the density distribution at $5t_{cc}$ and three small panels showing enlargements of the region of interaction between jet and cloud referred to density, temperature and the expansion velocity of emitting gas. The proper physical condition for emission are reached in a thin layer of compressed cloud material, whose width and mass grow in time as the shocked cloud material cools down.

The detailed physical properties of this line emitting region are reported in Fig. 5, where we have represented the behavior of density, temperature and velocity along radial cuts through this layer. We note that the proper conditions are matched in a layer of width $\lesssim 2\ pc$.

How the properties of the material contained in this thin layer compare with the physical conditions of gas of the NLR? To answer the question we plot in Fig. 6 the

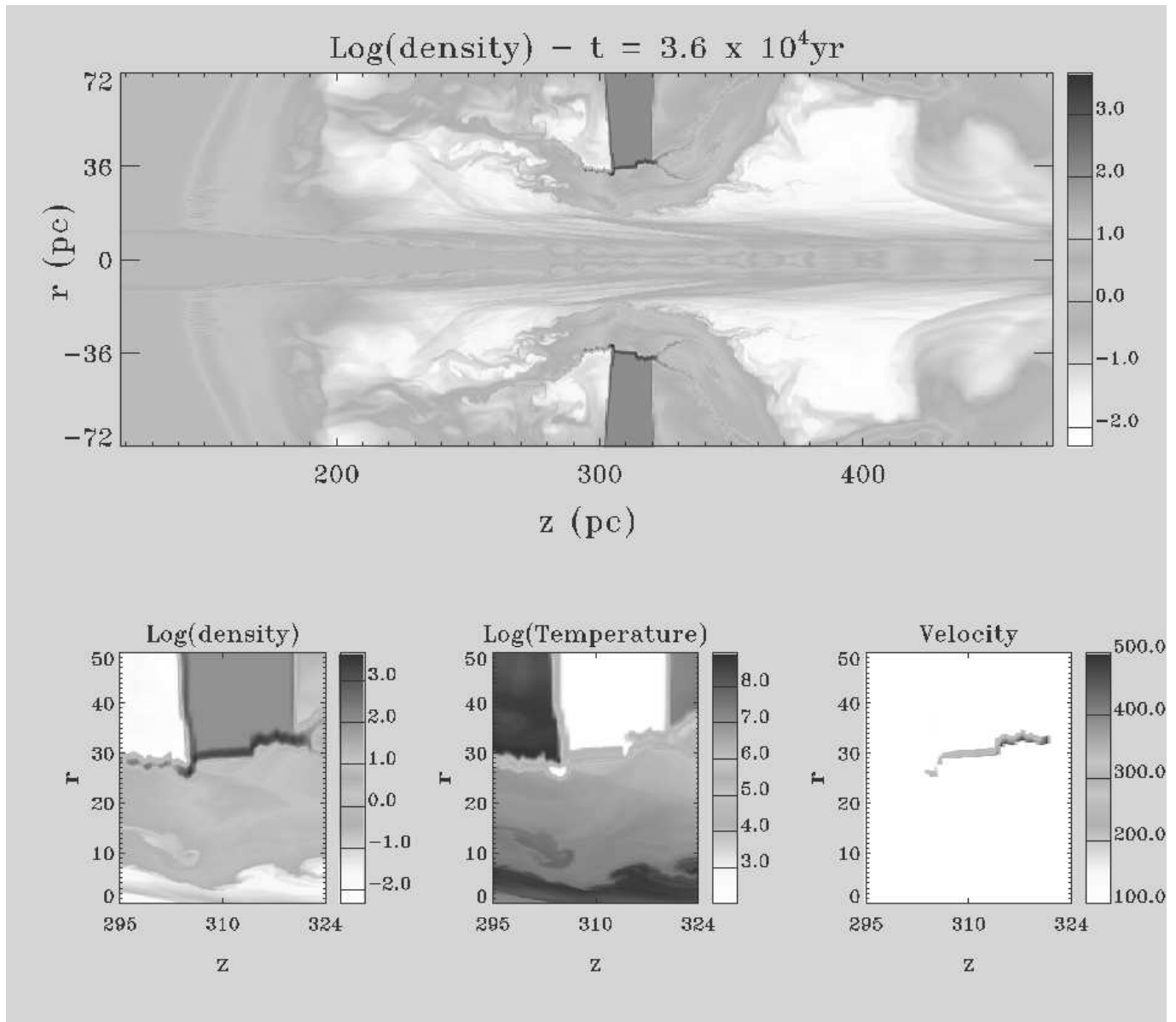


Fig. 4. The larger panel shows the image of the distribution of logarithm of density at $5t_{cc}$ for the case $\rho_{cloud} = 120 \text{ cm}^{-3}$, $v_{jet} = 32500 \text{ km s}^{-1}$. The other three small panels show, in enlargements of the interaction region, the distributions of the logarithm of density, the logarithm of temperature and of velocity.

temporal behavior of the mean expansion velocity (panel a) and mass (panel b) of the emitting material shell at two different density limits. We see that from the time when the jet touches the cloud until $2t_{cc}$, when a strong interaction between the jet head and the cloud takes place, the cloud material is accelerated and the quantity of emitting material increases; after this interval the jet flows, essentially freely, across the cloud without any further acceleration of the compressed material shell and the accelerated cloud material slows down monotonically. Notice that the mean expansion velocity, relative to an observer, lies, for the denser material, in the range $600 - 1200 \text{ km s}^{-1}$

(since one must consider twice the mean expansion velocity), that is in good agreement with the velocity deduced by the line widths detected. Looking more in detail at the emitting mass, we see that its growth begins some time after the jet has initiated to drill its way into the cloud, and this delay corresponds to the cooling time of the shocked material. We also note that, after $t = 2t_{cc}$, the jet continues to sweep out material laterally at a pace that is higher for the lighter material, the total mass exceeds $3 \times 10^4 / M_{\odot}$ at $t = 35,000 \text{ ys}$ and this would correspond to an H_{β} luminosity of $\sim 2 \times 10^{40} \text{ erg s}^{-1}$ which, considering also the

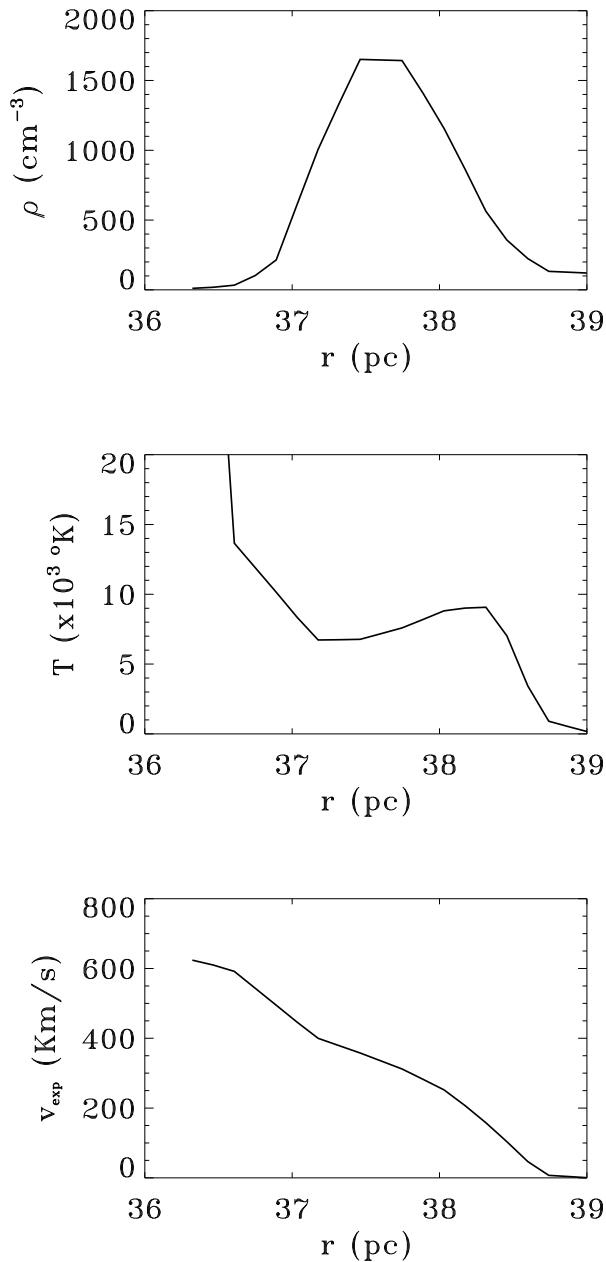


Fig. 5. The three panels present a transversal cut of density, temperature, and the expansion velocity, in the middle of cloud, across the thin emitting layer for the same case of Fig. 4. Notice that the coordinate r measure the distance from the jet axis.

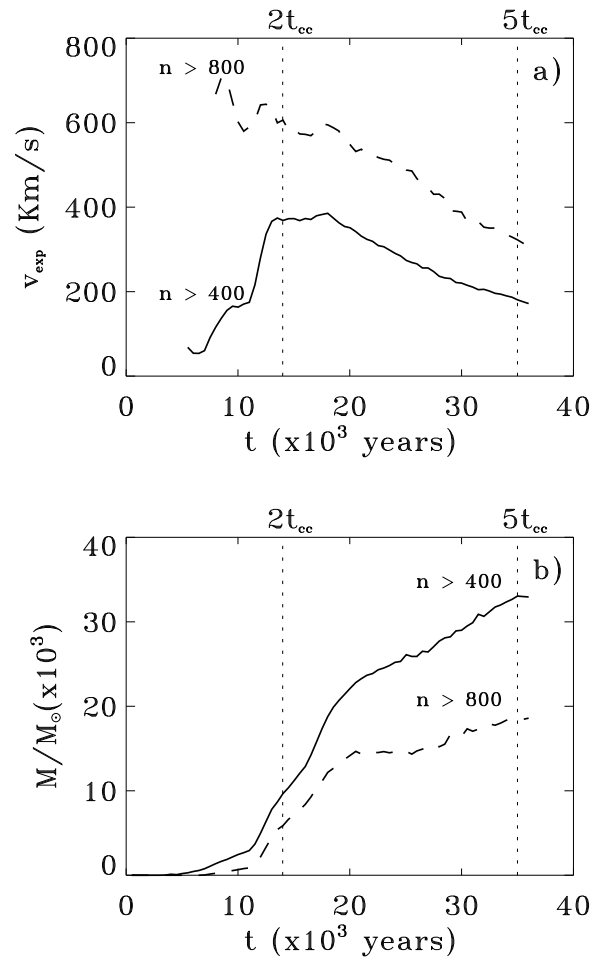


Fig. 6. In the two panels we plot the behavior of the mean expansion velocity of the emitting material vs time (panel a) and of the total emitting mass, in unit of solar masses, vs time (panel b). The solid lines refer to material denser than 400 particle per cube centimeter, while the dashed line refers to material denser than 800 particle per cube centimeter.

possibility of having simultaneously several active clouds, is consistent with the observed values.

As the interaction is effective over a timescale much longer than $t = t_{cc}$ the jet will quickly propagate into the low density inter-cloud medium and it will reach any other cloud lying on its path. Thus more than one cloud will be effectively interacting with the jet at any time. Each will display a behaviour typical of its evolutionary stage and the total emitting mass must be considered as the total over all clouds. Furthermore, this will naturally reproduce the jet-like morphology of the NLR.

5.2. Energetics

As discussed in the Introduction, the source of ionization of the NLR is still matter of debate. While the NLR gas is

Table 3. High frequency radiative power and radiative efficiencies

	$v_{jet} = 1,300 \text{ km s}^{-1}$	$v_{jet} = 6,500 \text{ km s}^{-1}$	$v_{jet} = 32,500 \text{ km s}^{-1}$
P_{kin}	$1.1 \cdot 10^{40} \text{ erg s}^{-1}$	$1.38 \cdot 10^{42} \text{ erg s}^{-1}$	$1.73 \cdot 10^{44} \text{ erg s}^{-1}$
$\rho_{cloud} = 30 \text{ cm}^{-3}$	$(P_{rad})_{max} = 0.03 \cdot 10^{40} \text{ erg s}^{-1}$ $\eta_{max} = 2.7\%$, $\eta_{2t_{cc}} = 0.08\%$	$(P_{rad})_{max} = 0.02 \cdot 10^{42} \text{ erg s}^{-1}$ $\eta_{max} = 1.6\%$, $\eta_{2t_{cc}} = 0.4\%$	$(P_{rad})_{max} = 0.07 \cdot 10^{42} \text{ erg s}^{-1}$ $\eta_{max} = 0.04\%$, $\eta_{2t_{cc}} = 0.5 \cdot 10^{-2}\%$
$\rho_{cloud} = 60 \text{ cm}^{-3}$		$(P_{rad})_{max} = 0.14 \cdot 10^{42} \text{ erg s}^{-1}$ $\eta_{max} = 10\%$, $\eta_{2t_{cc}} = 0.5\%$	$(P_{rad})_{max} = 0.15 \cdot 10^{42} \text{ erg s}^{-1}$ $\eta_{max} = 0.09\%$; $\eta_{2t_{cc}} = 4 \cdot 10^{-2}\%$
$\rho_{cloud} = 120 \text{ cm}^{-3}$		$(P_{rad})_{max} = 0.02 \cdot 10^{42} \text{ erg s}^{-1}$ $\eta_{max} = 1.4\%$, $\eta_{2t_{cc}} = 0.5\%$	$(P_{rad})_{max} = 0.35 \cdot 10^{42} \text{ erg s}^{-1}$ $\eta_{max} = 0.2\%$, $\eta_{2t_{cc}} = 1 \cdot 10^{-2}\%$

certainly illuminated by the nuclear source, its interaction with the radio jet also produces regions of high temperature and density which radiates ionizing photons. In this paragraph we derive the conversion efficiency of the jet kinetic power into energy radiated in ionizing photons. To estimate the ionizing energy flux we integrated radiative losses over all regions where $T > 10^5$ K as above this temperature most of them correspond to the production of photons with energy higher than the hydrogen ionization threshold.

In Table 3 we summarize our results reporting the kinetic power referred to the three different velocities ($P_{kin} = \rho v_{jet}^3 A$, where ρ , v_{jet} and A are respectively the density, the velocity and the transverse section of the jet) and the conversion efficiency at peak and after $2 t_{cc}$ for all the cases considered.

The peak efficiency reaches in one case a value as high as 10 % but it is usually 0.1 - 2 %. However, over the interaction, the typical value of η (well represented by its value after $2 t_{cc}$) is much lower $\eta \sim 10^{-4} - 5 \cdot 10^{-3}$. Faster jets have lower efficiency than slower jets and this conspires in producing a very similar amount of energy radiated in ionizing photons, $\sim 10^{40} \text{ erg s}^{-1}$, in all cases.

In Seyfert galaxies $L_{H\beta} \sim 10^{39} - 10^{42} \text{ erg s}^{-1}$ (Koski 1978). The minimum ionizing photon luminosity required to produce a given line emission luminosity corresponds to the limiting case in which all ionizing photons are absorbed and all photons have an energy very close to the hydrogen ionization threshold ν_{ion} . In this situation

$$L_{ion,min} = \frac{1}{p_{H\beta}} \frac{\nu_{ion}}{\nu_{H\beta}} L_{H\beta} \sim 50 L_{H\beta}$$

where $p_{H\beta} \approx 0.1$ is the probability that any recombination will result in the emission of an $H\beta$ photon.

It appears that, even in this most favourable scenario, the radiation produced in shocks can only represent a small fraction of the overall ionization budget of the NLR, particularly as sources with high radio luminosity (in which usually radio-jets are found) also have the highest line luminosity (e.g. Whittle 1985).

Nonetheless, in the most promising case examined above ($\rho_{cloud} = 120 \text{ cm}^{-3}$ and $v_{jet} = 32500 \text{ km s}^{-1}$) at the peak of the conversion efficiency the radiated energy is $3 \times 10^{41} \text{ erg s}^{-1}$ and it is substained over a crossing time, $\sim 10^4$ years. Shock ionization may thus produce important ionization effects which, however, can be only both local and transient.

6. Conclusions

We have studied in detail the dynamics of the interaction of a jet with a large cloud pre-existing in the ISM in order to find the conditions for which it is possible to reproduce the main physical parameters of the NLR emitting material.

Following the suggestion by Steffen et al. (1997b) that the most relevant effects of the interaction arise when a jet hits dense massive clouds, we adopted a quite simplified geometry of a single gas condensation with can be astrophysically identified with a giant molecular cloud. As the interaction last for a time considerably longer than the cloud crossing time more than one cloud will be interacting at any given time and they will display simultaneously

the different evolutionary stages of the interaction. Furthermore the characteristic jet-line structure of the NLR is thus reproduced. In any event, this case, i.e. the head-on collision with a large cloud, is the most efficient case of interaction, for the compression, acceleration and heating of the NLR material.

We concentrated our efforts on the exploration of the parameter plane (v_{jet} , ρ_{cloud}), since the other parameters, on which the simulation depends, have little influence on the properties of the optically emitting material. We have found that the condition for obtaining values of density, temperature and velocity in the observed range can be translated in a condition on the parameter τ , which is the ratio of the cloud crossing timescale to the radiative timescale ($0.3 < \tau < 0.55$) and which depends on our two fundamental parameters v_{jet} and ρ_{cloud} . For small values of τ , radiation is inefficient and it is not possible to produce regions dense enough, while, on the other hand, for large values of τ , the cloud is too dense and the obtained velocities are too low. We have explored a range of cloud densities which can be considered typical of GMCs and, for this range, the jet velocities span an interval from 4000 km s⁻¹ to 55,000 km s⁻¹.

The jet kinetic power corresponding to these combinations of parameters (for a jet density of 1 cm⁻³) ranges from 3.2×10^{41} to 8×10^{44} erg s⁻¹, in general agreement with the estimates of Capetti et al. 1999 for Mrk 3. For jet density much lower than 1 cm⁻³, however, in order to match the observed NLR conditions we would need a correspondingly higher velocity and therefore untenable requirements on the kinetic power which grows with v_{jet}^3 . We conclude that jets in Seyfert galaxies are unlikely to have densities much lower than 1 cm⁻³ and velocities higher than 50,000 km s⁻¹, and therefore they are very different from their counterparts in radio-galaxies in which densities are much lower and velocities are relativistic.

Concerning radio-galaxies we can speculate that with lower jet densities and higher velocities, the gas post-shock temperatures and radiative time would be increased with respect to the case of Seyfert galaxies and therefore the conditions for having efficient line emission would be more difficult to meet. In addition the different properties of the jet environment in the elliptical galaxies hosting radio-galaxies render encounters with gas condensations less likely to occur. This probably explain why the association between radio and line emission although often present in radio-galaxies (e.g. Baum and Heckman 1989) is not as strong as in Seyfert galaxies.

Finally, the study of the global dynamics allowed us to have estimates of the overall efficiency of the conversion of kinetic to high frequency radiative power in the shocks that form in the interaction between jet and ambient medium. We have found that the efficiency is increased by the presence of the cloud, its peak value is 0.1 - 2 % , its typical value is much lower $\sim 10^{-4} - 5 \times 10^{-3}$ and it decreases with the jet power. These results lead us to the

conclusion that radiation emitted in shocks can be only a small fraction of the overall ionization budget of the NLR, although it can have local and transient important effects.

Acknowledgements. We thank CNAA (Consorzio Nazionale per l'Astronomia e Astrofisica) for supporting the use of supercomputers at CINECA, .

References

- Allen M.G., Dopita M.A., Tsvetanov Z.I., Sutherland R.S., 1999, ApJ 511, 686
- Antonucci R.R.J., 1993, ARA&A, 31, 473
- Axon D.J., Capetti A., Macchetto F.D., 1999, ApJ submitted
- Axon D.J., Marconi A., Capetti A., Macchetto F.D., Schreier E., Robinson, A., 1998, ApJ 496, L75
- Baum S.A., Heckman T., 1989, ApJ 336, 702
- Blitz L., 1993, in Protostars and Planets III, eds. E.H. Levy and J.I. Lunine, Tucson: Univ. of Arizona Press, p. 125
- Bodo G., Massaglia S., Rossi P., Rosner R., Malagoli A., Ferrari A., 1995, A&A 303, 281
- Caganoff S., et al., 1991, ApJ 377, L9
- Capetti A., Axon D.J., Macchetto F.D., Marconi A., Winge C., 1999, ApJ, 516, 187
- Capetti A., Axon D.J., Macchetto F.D., 1997, ApJ 487, 560
- Capetti A., Axon D. J., Macchetto F.D., Sparks W.B., Boksenberg, A. 1996, ApJ 469, 554
- Capetti A., Macchetto F.D., Axon D.J., Sparks W.B., Boksenberg, A. 1995, ApJ 448, 600
- Capetti A., Axon D.J., Kukula M., Macchetto F.D., Pedlar A., Sparks W.B., Boksenberg A. 1995, ApJL 454, L85
- Cioffi D. F., Blondin J. M., 1992, ApJ 392, 458
- Colella P., Woodward P.R., 1984, J. Comp. Phys. 54, 174
- Cox D.P., Reynolds R.J., 1987, ARA&A 25, 303
- Dopita M.A., & Sutherland R.S., 1995, ApJ 455, 468
- Dopita M.A., & Sutherland R.S., 1996, ApJS 102, 161
- Evans I. , Koratkar A. , Allen M. , Dopita M., Tsvetanov Z., 1999, ApJ 521, 531
- Falcke H., Wilson A.S., Simpson C., Bower G.A., 1996, ApJ 470, 31
- Falcke H., Wilson A.S., Simpson C. 1998, ApJ 470, 31
- Ferruit P. , Wilson A. S., Whittle M. , Simpson C. , Mulchaey J. S., Ferland G. J., 1999, ApJ 523, 147
- Koski A. T., 1978, ApJ 223, 56
- Kraemer S. B., Ruiz J. R., Crenshaw D. M., 1998, ApJ 508, 232
- Kukula M., Pedlar A., Baum S., O'Dea C.P., 1995, MNRAS 276, 1262
- Kukula M., Ghosh T., Pedlar A., Schilizzi R.T., 1999, ApJ 518, 117
- Norman M. L., Winkler K. -H. A., Smarr L., Smith M. D., 1982, A&A 113, 285
- Pedlar A., et al. 1993, MNRAS 263, 471
- Raymond J. C., & Smith B. W., 1977, ApJS 35, 419
- Rossi P. & Capetti A., 1998 in "Astrophysical Jets: Open Problems", eds. Massaglia S. & Bodo, G., New York: Gordon and Breach, p.139
- Steffen W., Gomez J. L., Williams R. J. R., Raga A. C., Pedlar A., 1997a, MNRAS 286, 1032
- Steffen W., Gomez J. L., Raga A. C., Williams R. J. R., 1997b, ApJ 491, L73

- Sutherland R.S., Bicknell G.V., Dopita, M.A., 1993, ApJ 414,
510
- Whittle M., 1985, MNRAS 213, 1
- Wilson A.S., & Tsvetanov Z.I., 1994, AJ 107, 1227
- Wilson A. S., & Raymond J. C., 1999, ApJ 513, L115